

# COUNTER-HAIRPIN VORTICES IN THE WAKE OF A SHARP TRAILING-EDGE

**Sina Ghaemi**

Department of Aerodynamics  
Delft University of Technology  
Kluyverweg 1, 2629 HS, Delft  
s.ghaemi@tudelft.nl

**Fulvio Scarano**

Department of Aerodynamics  
Delft University of Technology  
Kluyverweg 1, 2629 HS, Delft  
f.scarano@tudelft.nl

## ABSTRACT

The unsteady organization and the evolution of the coherent structures within the immediate wake of the sharp symmetric trailing-edge of a NACA0012 airfoil is investigated using two-component (2C) and tomographic particle image velocimetry (Tomo-PIV). The inspection of the Tomo-PIV results showed new vortical structures, introduced here as counter-hairpin vortices, evolve in the wake region to direct the turbulent mechanism towards recovery of the wake deficit. These vortical structures are topologically similar to the hairpins of a turbulent boundary layer as they appear to be U-shaped but with inverted orientation. The spanwise portion of a counter-hairpin vortex is in the vicinity of the wake centerline and the legs are inclined at an approximately 60 degree to the wake axis in the downstream direction. They partially wrap around the high speed streaks and frequently sweep the high-speed flow towards the wake centerline. A pattern recognition algorithm is applied to establish characterization based on an ensemble averaged counter-hairpin vortex. The formation mechanism of the counter-hairpin vortices is attributed to the shear layer produced along the wake centerline by the neighboring of a low and a high speed streak which promotes formation of spanwise vortices that form the vortex by connection to quasistreamwise vortices.

## INTRODUCTION

The turbulent flow of the immediate wake is highly considered in the design process of the wing, high-lift devices, and the engine fan of aircrafts. The turbulent fluctuations within this region affect the pressure distribution around the airfoil and result in unsteady loads and structural vibrations (Sharland 1964). The trailing-edge noise which includes the noise of the wing, high-lift devices, blades and the outlet guide vanes of aircraft engine (Brouwer & Rienstra 2008) is also due to the acoustic scattering of the turbulent fluctuations in the vicinity of the trailing-edge (Ffowcs Williams & Hall 1970).

The broadband component of the trailing-edge noise is associated to a non-periodic wake and is generated over a wide range of frequencies by the acoustic scattering from the sudden distortion of vortical structures of different length scales (Sandberg & Sandham 2008). The contributing turbulent aspects are complex and linked to the turbulent boundary layer upstream of the trailing-edge.

The profiles of statistical quantities of the wake such as mean and fluctuating velocity have similar trend with respect to the upstream turbulent boundary layer (Haji-Haidari & Smith 1988). The length scales available in the wake and the upstream boundary layer are also of the same order of magnitude. After the trailing-edge, the production of turbulence further persists in the immediate wake as there is still considerable  $u$  and  $v$  correlation (Andreopoulos & Bradshaw 1980). The existence of the logarithmic trend along the wake centerline in the intermediate wake region (Haji-Haidari & Smith 1988) also indicates the possibility of self-similar structures with a hierarchy of length-scale in the wake region. These features suggests similarities between the coherent structures of the two boundary layer and the subsequent wake. However, there are also distinguishing features between the structures of the two regions.

The net transport of momentum within the wake region is oriented towards the wake centerline to recover the wake deficit (Andreopoulos & Bradshaw 1980). This is in contrary to a fully developed turbulent boundary layer as it is dominated by ejection events that transport momentum away from the wall vicinity resulting in further growth of the boundary layer thickness. Therefore, the vortical structures which carry out the dominant transport of momentum within the wake region act in an opposite direction to those of the turbulent boundary layer. These vortical structures are speculated to result in occasional positive  $u$  fluctuations at the edge of the inner wake that transport fluid towards the wake centerline (Andreopoulos & Bradshaw 1980). Haji-Haidari & Smith (1988) resembled these inward moving fluid to sweep events of a turbulent boundary layer and associated them to

streamwise vortices. However, the characteristics of these vortical structures are still unclear.

The current work aims to tackle the detailed flow physics in the immediate wake of the sharp trailing-edge of a non-lifting airfoil and identify the unsteady organization of the flow coherent structures and their evolution. The difficulties in identifying the spatio-temporal organization of the coherent structures are overcome in this work by applying a state-of-art time-resolved Tomo-PIV (Elsinga et al. 2006) which is a three-dimensional extension of standard PIV technique.

## EXPERIMENTAL APPARATUS AND PROCEDURES

An open-test-section open-loop wind tunnel with a cross-section of  $0.40 \times 0.40 \text{ m}^2$  was used to conduct the experiments. The original NACA0012 of  $C=0.4 \text{ m}$  chord length and  $14^\circ$  total angle at the trailing-edge has been modified by extending the trailing-edge  $4 \text{ mm}$  in the chordwise direction to reduce the trailing-edge thickness to  $h=0.2 \text{ mm}$  and mitigate vortex shedding. The airfoil was installed at zero angle-of-attack spanning the entire test section. The laminar-to-turbulent transition of the boundary layers on both sides of the airfoil were forced with a zig-zag strip to ensure spanwise uniform boundary layer properties. The zig-zag element is  $0.5 \text{ mm}$  thick with a pitch of  $6 \text{ mm}$  and was located at  $0.25C$  from the airfoil leading-edge. At a free stream velocity of  $U_\infty=14 \text{ m/s}$ , the chord-based Reynolds is  $Re_c=386000$  and that based on momentum thickness is  $Re_\theta=1300$  at  $20 \text{ mm}$  upstream of the trailing-edge. The coordinate systems as shown in Figure 1 is compatible with the wake centerline. The boundary layer thickness ( $\delta_{99}$ ), the displacement thickness ( $\delta^*$ ), and the momentum thickness ( $\theta$ ) at  $s = -20 \text{ mm}$  upstream of the trailing-edge are  $10.1, 2.2, 1.4 \text{ mm}$ , respectively.

A 2C-PIV system has been applied to investigate the turbulent statistics. A Quantronix Darwin-Duo laser system with average output of  $80 \text{ W}$  is applied to form a laser sheet of approximately  $1 \text{ mm}$  thickness. The illuminated region is imaged by a Photron Fast CAM SA1 with a 12 bit CMOS sensor of  $1024 \times 1024$  pixels (pixel pitch  $20 \mu\text{m}$ ). The camera was equipped with a Nikon objective of  $105 \text{ mm}$  focal length set to aperture of  $f\# = 2.8$ . Wall-normal streamwise field-of-view (FOV) of  $52.3 \times 52.3 \text{ mm}^2$  is considered. Ensembles of 1000 double-frame recordings with  $42 \mu\text{s}$  pulse separation at acquisition frequency of  $100 \text{ Hz}$  have been acquired. The velocity fields are obtained from individual correlation maps by windows of  $16 \times 16$  pixels and  $50\%$  overlap processed in Davis 7.4 (LaVision).

Quantitative flow visualization is conducted using Tomo-PIV technique to assess the flow coherent structures. This method is a 3D extension of planar (stereoscopic) PIV and was developed by Elsinga et al. (2006). The measurement setup consists of the same base equipment (laser, cameras, lens objective) as the 2C-PIV system. The higher light demand of the Tomo-PIV experiment was fulfilled using a multi-pass light amplification system (Ghaemi & Scarano 2010). The imaging system consists of four Photron Fast CAM cameras aligned along the wall-normal spanwise plane

with respect to the airfoil as illustrated in Figure 1. The cameras are equipped with Scheimpflug adapters and  $105 \text{ mm}$  objectives. The aperture of the two side cameras (1 and 4) is set to  $f\#=22$  while the two middle cameras (2 and 3) image at  $f\#=16$ . The four cameras and the laser have been synchronized to record double-frame images with  $42 \mu\text{s}$  laser pulse separation at  $100$  and  $2700 \text{ Hz}$  using High Speed Controller (LaVision). The flow is seeded with the  $1 \mu\text{m}$  droplets to obtain a concentration of  $4 \text{ particles/mm}^3$ , resulting in a source density of approximately  $0.065$  particles per pixel in the images corresponding to the measurement volume of  $47 \times 47 \times 8 \text{ mm}^3$ .

The data analysis has been conducted by the LaVision software Davis 7.4 on a 8-cores PC. The reconstructed volume was discretized at  $22 \text{ voxels/mm}$ . Interrogation volumes of  $32 \times 32 \times 32$  voxels with  $75\%$  overlap have been considered enclosing approximately  $13$  particles. The vector field is a volume of  $128 \times 128 \times 22$  vectors each spaced  $0.37 \text{ mm}$  away from the neighboring vectors and is calculated by cross-correlation adopting a multi-grid volume-deformation method.

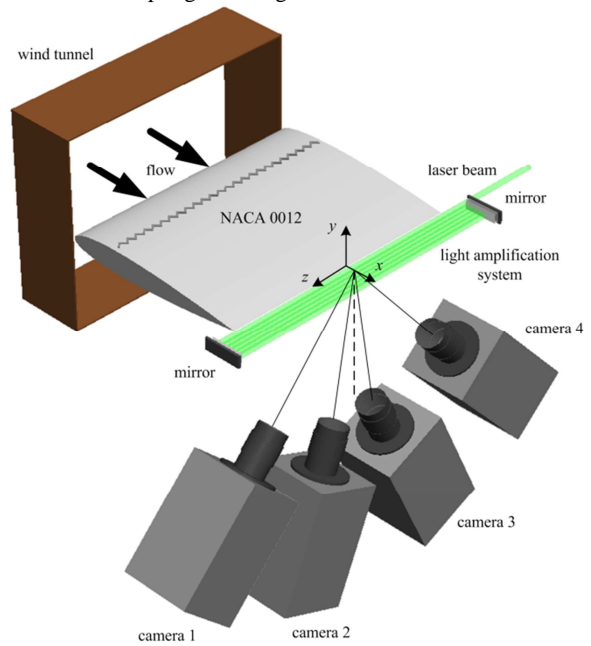


Figure 1. The arrangement of the cameras, airfoil, and the multi-path illumination system in the Tomo-PIV experiment.

The detection of relevant features exhibiting a vortex-like instantaneous flow topology is performed by means of pattern recognition analysis (PRA). The approach follows that used by Ferré & Giralt (1989) and later modified for PIV measurements by Scarano et al. (2000). The working principle relies on the choice of an indicator function and on the formulation of a spatial template. For this purpose a-priori knowledge about the flow properties is required. The indicator function for the wake region is considered as a combination of a counter-hairpin vortex which has a reverse topology with respect to a hairpin vortex of a turbulent

boundary layer and encloses a sweep event satisfying  $u > 0$  and  $v < 0$  (see Figure 2). As it will be discussed in the remainder this indicator is anticipated by visual inspection of the Tomo-PIV snapshot and is followed by verification through the algorithm.

The spatial template follows an arc-like vortex pattern visualized by the Q-criterion (Hunt et al. 1988) based on the second eigenvalue of the velocity gradient tensor. The main parameters governing the topology are the width between legs  $l$ , and the height  $h$  indicated in Figure 2. In the present case a value of  $l = 120^+$  (3.6 mm) is chosen in accordance with the Tomo-PIV visualizations which is also consistent with the typical width of the low/high speed streaks (Head & Bandyopadhyay 1981). From the observations, it emerges that the vortex axis in the head region has a significant flatness which is considered with a 4th order polynomial for the vortex line. The curve describing the vortex line topology is given by

$$\begin{cases} x = \frac{1}{a}z^4 \cos\alpha \\ y = \frac{1}{a}z^4 \sin\alpha \end{cases}$$

where the constant  $a$  depends on the wake half-width and in this case is set to  $a = 5 \text{ mm}^3$  (equivalent to  $(167^+)^3$ ). The angle  $\alpha$  is the orientation of the vortex with respect to the streamwise direction and is selected as  $\alpha = 60^\circ$ . The embedded sweep event is generated by applying  $-uv/U_\infty = 0.01$  (satisfying  $u > 0$  and  $v < 0$ ) within an ellipsoid defined by

$$\frac{x^2}{a_x^2} + \frac{y^2}{a_y^2} + \frac{z^2}{a_z^2} = 1$$

The constants are set as  $a_x = 1.5 \text{ mm}$  ( $50^+$ ),  $a_y = 3.5 \text{ mm}$  ( $117^+$ ), and  $a_z = 3.5 \text{ mm}$  ( $117^+$ ).

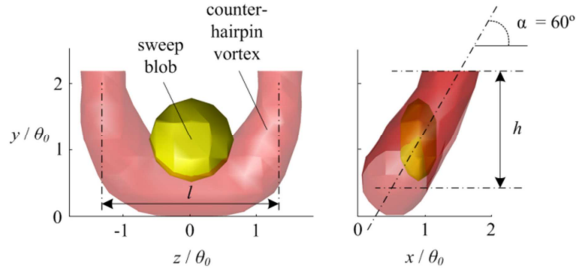


Figure 2. The reference structure for the wake region. The red iso-surface shows the vortex surface at  $Q = 1e6 \text{ 1/s}^2$  while the yellow iso-surfaces indicates a sweep event ( $u > 0$  and  $v < 0$ ) of  $-uv/U_\infty = 0.008$  strength.

## STATISTICAL ANALYSIS

The profiles of Reynolds stress  $12\theta_0$  prior to the trailing-edge shown in Figure 3 (left) demonstrate similar trend relative to those of a fully developed turbulent boundary layer (Spalart 1988). The solid surface results in lower wall normal fluctuations,  $\langle v^2 \rangle$ , in comparison to streamwise fluctuations,  $\langle u^2 \rangle$ . The shear stress  $\langle uv \rangle$  is mainly associated to ejection events induced by hairpin vortices (Wallace et al. 1972). The behavior of  $\langle u^2 \rangle$ ,  $\langle v^2 \rangle$ , and  $\langle uv \rangle$  at  $x/\theta_0 = 12$  of the wake

region resembles those of the upstream turbulent boundary layer with approximately the same intensity. The maximum of the  $\langle uv \rangle$  is at  $y/\theta_0 \approx 3$ , consequently, the net force exerted by the Reynolds shear stress,  $d(-\rho\langle uv \rangle)/dy$ , is negative and uniform above this point and positive below it. While the negative force of the outer layer decelerates the mean velocity, the positive force of the inner wake accelerates the flow and acts towards filling the velocity deficit at the wake centerline. The disappearance of the wall results in the rapid intensification of the  $\langle v^2 \rangle$  fluctuations (close to the centerline) relative to the upstream boundary layer. The near wall peak in the  $\langle u^2 \rangle$  profile of the boundary layer has also vanished in the wake as the high gradient of the near wall velocity profile has been recovered within a few  $\theta_0$  from the trailing-edge. At  $x/\theta_0 = 12$  and on the centerline  $\langle u^2 \rangle = 1.1\langle v^2 \rangle$  showing the development towards isotropic state.

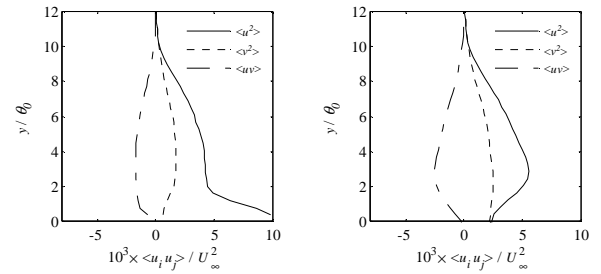


Figure 3. normal and shear Reynolds stress in the turbulent boundary layer at  $12\theta_0$  upstream of the trailing-edge and (right) along the centerline of the wake at  $x/\theta_0 = 12$  (right).

The direction of transport of turbulent kinetic energy by velocity fluctuations before and after the trailing-edge is investigated using the triple products as shown Figure 4 (left) and (right), respectively. The negative values of  $\langle u^3 \rangle$  and positive  $\langle uv^2 \rangle$  within the boundary layer indicate that the turbulent kinetic energy embedded in  $\langle u^2 \rangle$  is transported dominantly via negative  $u$  and positive  $v$  fluctuations. The  $\langle uv^2 \rangle$  and  $\langle v^3 \rangle$  products are also negative and positive, respectively, which also indicates dominate transport of  $\langle v^2 \rangle$  through negative  $u$  and positive  $v$  fluctuations. It is known that  $u < 0$  and  $v > 0$  fluctuations are associated to ejection events within a turbulent boundary layer (Corino & Brodkey 1969). The triple products of turbulent fluctuations in Figure 4 (right) show a similar behavior, i.e.,  $u < 0$  and  $v > 0$ , within the outer wake region ( $y/\theta_0 > 3$ ). Therefore, the ejection events of the boundary layer further persist into the outer layer of the wake and dominate the transport of turbulent kinetic energy. Instead, in the inner wake ( $y/\theta_0 < 3$ ) an opposite trend is observed. Positive  $\langle u^3 \rangle$  and negative  $\langle uv^2 \rangle$  indicate that the turbulent kinetic energy embedded in  $\langle u^2 \rangle$  is transported dominantly via positive  $u$  and negative  $v$  fluctuations. The  $\langle uv^2 \rangle$  and  $\langle v^3 \rangle$  products are also positive and negative respectively which also point out major transport of turbulent kinetic energy of  $\langle v^2 \rangle$  through positive  $u$  and negative  $v$  fluctuations. If these  $u$  and  $v$  fluctuations are correlated they form a sweep event observed as intrushes of flow towards the

wake centerline by the hydrogen bubble visualization of Haji-Haidari & Smith (1988). Andreopoulos & Bradshaw (1980) have demonstrated using temperature-conditioned sampling that the sweep events transport unmixed fluid of the incoming turbulent boundary layers towards the centerline.

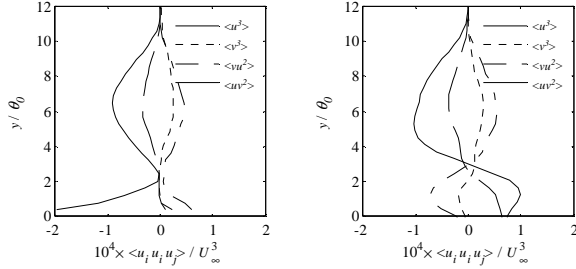


Figure 4. triple products of turbulent fluctuations at  $12\theta_0$  upstream of the trailing-edge (left) and along the centerline of the wake at  $x/\theta_0=12$  (right).

The quadrant splitting identifies the contribution of the ejection and sweep events to the total mean values of kinetic energy and Reynolds stress. The  $u$  and  $v$  within the boundary layer demonstrate co-existence of ejection (Q2 quadrant) and sweep (Q4 quadrant) events within the log-layer of the boundary layer as shown in Figure 5 (left). Along the wake centerline the major correlation between  $u$  and  $v$  fluctuations is observed as sweep events occupying both Q4 and Q1 quadrants of Figure 5 (right) since they are generated by both sides of the wake centerline. The Q4 sweep events transport the unmixed flow (Andreopoulos & Bradshaw 1980) of the upper boundary layer ( $y > 0$ ) downwards to the wake centerline while the Q1 transport the unmixed flow of the lower boundary layer ( $y < 0$ ) up towards the centerline. The ejection events along the centerline are weaker in strength. Therefore, the sweep events transport the unmixed fluid into the inner layer enhancing the recovery of the wake deficit. Yet, the vortical structures responsible for the sweeps along the wake centerline are to be specified.

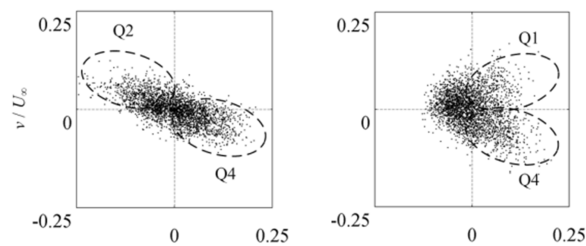


Figure 5. Quadrant analysis within the boundary layer at  $1.1\theta_0$  wall normal location and  $12\theta_0$  upstream of the trailing-edge (left) and along the wake centerline at streamwise location of  $x/\theta_0=3.5$  (right).

## UNSTEADY FLOW ORGANIZATION

The sudden disappearance of the solid wall adds another degree of interaction between the low and high speed streaks. The uncorrelated turbulent fluctuations of the two boundary layers before the trailing-edge result in three possible combinations of high-high (HH), low-low (LL), and low-high (LH) speed streaks in the  $xy$  plane as show in Figure 6. The streaks of LL and HH combinations have merged along the centerline and show least vortical activity along their interface. On the other hand, the LH arrangement shows significant vortical activities at the streaks interface along the centerline. The nature of these vortical activities is scrutinized in Figure 7 in which a 3D representation of the high speed streak and the surrounding vortical structures of the LH cross section of Figure 6 (right) is illustrated. It is observed that the spanwise rolls of  $\omega_z$  vorticity at the wake centerline between the high and low speed streaks are further extended by quasistreamwise vortices forming U-shape structures. These vortical structures are introduced here as *counter-hairpin* vortices and are oriented in an opposite orientation with respect to the hairpin vortices of a turbulent boundary layer since the spanwise part (vortex head) is at the low velocity region of the mean velocity profile (wake centerline) while the quasi-streamwise parts (the legs) are stretched away. The spanwise portion of counter-hairpins has the same vorticity direction as that of the hairpin vortices ( $\omega_z < 0$ ) making it rather difficult to be distinguished with point-wise or even planar measurements of the previous investigations. The visualization at the right side of Figure 7 shows that the counter-hairpin vortices induce a focused sweep event while a weak ejection region covers the outbound of the vortices. Andreopolous & Bradshaw (1980) have previously observed occasional positive  $u$  fluctuations at the edge of the inner wake and speculated those to be the result of the inward motion of the outer-region fluid towards the wake centerline. Later Haji-Haidari & Smith (1988) resembled these inward moving fluid to sweep events of a turbulent boundary layer and associated them to streamwise vortices inducing non-periodic intrushes of the outer fluid towards the wake centerline. However, the spanwise portion of these vortices have escaped their hydrogen bubble visualization and the complete vortex structure could not be identified. The Tomo-PIV visualization of this work shows that the counter-hairpin vortices generate focused sweeps of the high speed fluid within the wake towards the centerline promoting the recovery of the wake deficit.

The vortical structures within the wake region can be distinguished from those of the boundary layer by their accumulation around the high speed streaks as observed in the instantaneous Tomo-PIV snapshot of Figure 8. Two samples of the counter hairpin vortices are also specified with a pronounced U-shape structure. The magnified views also demonstrated the embedded sweep event in the centroid of these vortices while the surrounding ejection event appears irregular and weak. The occurrence probability of a complete counter-hairpins as shown in Figure 8 is relatively low which necessitates a systematic education.

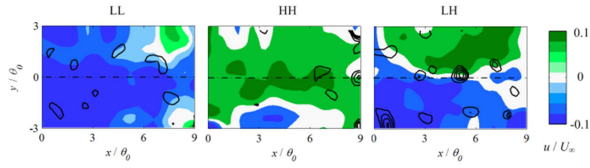


Figure 6. The interface between three combinations of low-low (LL), high-high (HH), and low-high (LH) interfaces. The solid contours show spanwise vortex cores identified by swirling strength  $\lambda_{cj}$  (Tomkins & Adrian 2003).

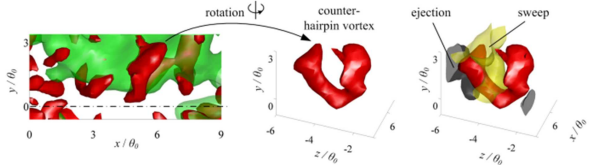


Figure 7. 3D visualization of the vortical structures (red,  $Q = 0.8e6 \text{ 1/s}^2$ ) wrapped around a high speed streak. The sweep (yellow) and ejection (black) regions are identified by  $-uv/U_\infty^2=0.01$  and  $-uv/U_\infty^2=0.001$ , respectively.

The ensemble averaged counter-hairpin vortices is shown by iso-surface of  $Q = 0.5e6 \text{ 1/s}^2$  in Figure 9. The analysis confirms existence of counter-hairpin vortices in the wake region in a large realization set and demonstrates mean kinematic features of the vortex structure. The average counter hairpin has a height and leg spacing of  $2\theta_0$  ( $95^\circ$ ). The inclination angle is  $60$  degree with respect to the streamwise direction. A focused sweep of the fluid is shown following the streamlines. The streamlines demonstrate higher curvature around the spanwise portion of the vortex due to higher vorticity of this region. The sweep event is identified with an isosurface of  $-uv/U_\infty^2=0.004$  showing a focused sweep of high speed flow at the centroid of the counter hairpin vortex. The ejection event is visualized at 20 times lower strength ( $-uv/U_\infty^2=0.0002$ ) relative to the sweep event and covers the outboard of the vortex.

The formation mechanism of the counter-hairpin vortices can be explained through the 3D organization of the low and high speed streaks in the wake region. The high speed streak of the wake region similar to those of the turbulent boundary layer, are adjacent to low speed streaks in the spanwise direction which ensures existence of enough shear to supply the legs of the counter hairpin vortices. However, the spanwise section of the counter-hairpin vortex also depends on existence of velocity difference at the wake centerline. Investigation of the Tomo-PIV snapshots shows that this condition can be met by simultaneous arrival of a high and a low speed streak from the two sides of the trailing-edge. The cross-sectional view of Figure 10 shows the  $u$  fluctuation in a  $yz$  plane crossing through a counter hairpin vortex in the wake region. The high speed streak embedded in the centroid of the counter hairpin vortex is in contact with a low speed streak on the other side of the centerline while it is also surrounded by two low speed streaks on the spanwise sides to promote formation of a counter hairpin vortex.

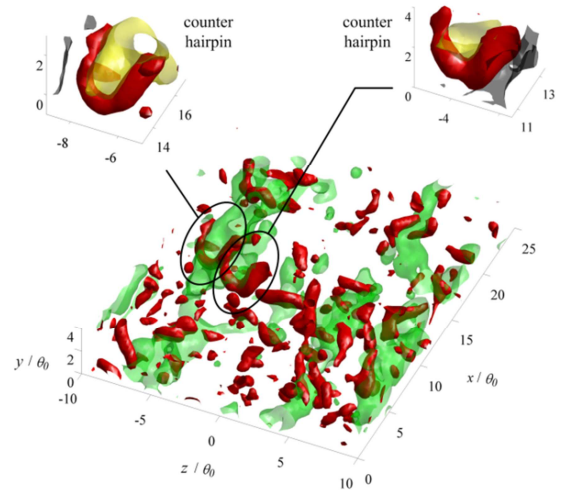


Figure 8. 3D organization of vortical structures (red,  $Q = 0.8e6 \text{ 1/s}^2$ ) and the high speed streaks (green,  $u/U_\infty = 0.1$ ) within the wake region. Two samples of counter hairpin vortices along with the sweep ( $-uv/U_\infty^2 = 0.003$ , yellow) and ejection ( $-uv/U_\infty^2 = 0.0015$ , black) events are identified.

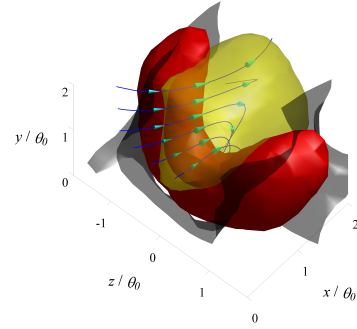


Figure 9. Ensemble averaged counter hairpin vortex obtained from PRA. The vortex (red) is identified at  $Q = 0.5e6 \text{ 1/s}^2$  while the sweep (yellow) and the ejection (gray) events are identified by  $-uv/U_\infty^2 = 0.0002$  and  $0.004$ , respectively. The streamlines are relative to  $U = 0.66U_\infty$ .

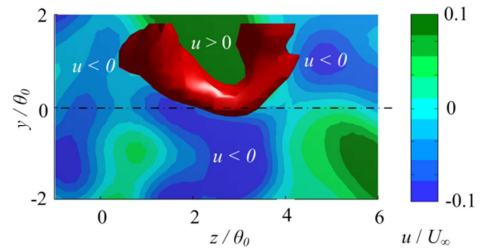


Figure 10. Cross section of  $u$  fluctuations across a counter-hairpin vortex.

A time sequence of the formation mechanism of a counter-hairpin vortex is shown in Figure 11. The first cross section at  $t_0$  corresponds to  $5\theta_0$  upstream of the trailing-edge where two quasistreamwise vortices (hairpin legs) are observed on the

two sides of a high-speed streak. At  $x/\theta_0=3$  after the trailing-edge, the quasistreamwise vortices start to be connected by a spanwise portion (head of the counter-hairpin). At this moment, the vortex is highly distorted as the legs arrive at the trailing-edge with slight delay and different orientation. The head and the two legs further unify at downstream location of  $x/\theta_0=12$  and form a more regular counter-hairpin shape. Based on this evidence the formation mechanism of counter-hairpin vortices is realized by connection between two quasistreamwise vortices advected into the wake. The connection is a spanwise vortex in the vicinity of the centerline formed by the shear resulted from a low speed flow on the other side of the wake centerline.

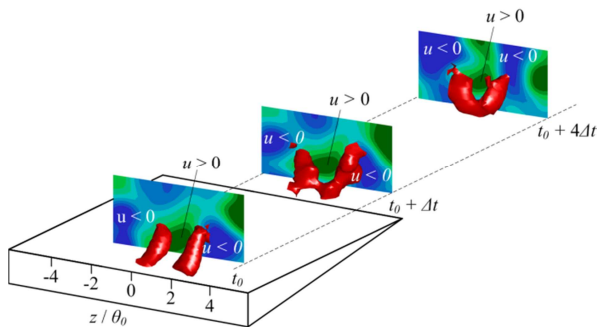


Figure 11. Time sequence of formation of a counter hairpin vortex. The visualization shows vortices identified by isosurfaces of  $Q = 0.8e6 \text{ 1/s}^2$  along with spanwise-wall normal plane of  $u$  fluctuations (similar to Figure 10).

## CONCLUSION

The analysis of triple products of turbulent fluctuations and the quadrant splitting of turbulent fluctuations confirmed that the net direction of transport of momentum and turbulent kinetic energy within the inner wake follows the sweep events towards the wake centerline. The Tomo-PIV visualization revealed that the sweep events are generated by vortices named here as counter-hairpin vortices. The counter-hairpin vortices are topologically similar to the hairpins but with an opposite orientation and function. The spanwise portion is located close to the wake centerline and the two attached quasistreamwise vortices are stretched outward with 60 degree angle with respect to the free stream direction. The counter-hairpin vortices partially surround the high speed streaks in contrary to the hairpin vortices that surround the low speed streaks in a turbulent boundary layer. The centroid of a counter-hairpin vortex embeds a concentrated region of sweep event which transports the high speed fluid and turbulent kinetic energy towards the wake centerline promoting recovery of the wake deficit. The investigations showed that the counter-hairpin vortices are formed as a result of the formation of spanwise vortices along the wake centerline upon disappearance of the solid wall. The sudden vanishing of the wall allows interaction of low and high speed streaks emerging from the two sides of the trailing-edge forming

regions of high shear if a low and high speed streak appear on the two sides of the wake centerline.

This work was conducted as a part of the FLOVIST project (Flow Visualization Inspired Aeroacoustics with Time Resolved Tomographic Particle Image Velocimetry), funded by the European Research Council (ERC), grant no 202887.

## REFERENCES

- Andreopoulos, J. & Bradshaw, P. 1980 Measurements of interacting turbulent shear layers in the near wake of a flat plate. *J Fluid Mech.* 100, 639-668.
- Brouwer, H.H. & Rienstra S.W. 2008 Aeroacoustics research in Europe: The CEAS-ASC report on 2007 highlights, *Journal of Sound and Vibration* 318, 625-654.
- Corino, E. R. & Brodkey, R. S. 1969 A Visual Investigation of the Wall Region in Turbulent Flow, *J. Fluid Mech.* 37, 1-30.
- Elsinga, G. E., Scarano, F., Wieneke, B. & van Oudheusden B. W. 2006 Tomographic particle image velocimetry, *Exp. Fluids* 41, 933-947.
- Ferré J. A. & Giralt F. 1989 Pattern-recognition analysis of the velocity field in plane turbulent wakes. *J Fluid Mech.* 198, 27-64.
- Ffowcs Williams, J. E. & Hall, L. H. 1970 Aerodynamic sound generation by turbulent flow in the vicinity of a scattering half plane, *J. Fluid Mech.* 40, 657-670.
- Ghaemi, S. & Scarano F. 2010 Multi-pass light amplification for tomographic particle image velocimetry applications *Meas. Sci. Technol.* 22, 5pp
- Haji-Haidari, A. & Smith, C. R. 1988 Development of the turbulent near wake of a tapered thick flat plate. *J Fluid Mech.*, 189, 135-163.
- Head, M. R. & Bandyopadhyay P. 1981 New aspects of turbulent boundary-layer structure. *J Fluid Mech.*, 107, 297-338.
- Hunt, J. C. R., Wray, A. A. & Moin, P. 1988 Eddies, stream, and convergence zones in turbulent flows. *Center for Turbulence Research Report* CTR-S88, 193-208
- Sandberg, R. D. & Sandham, N. D. 2008 Direct numerical simulation of turbulent flow past a trailing edge and the associated noise generation, *J. Fluid Mech.* 596, 353-385.
- Scarano, F. & Reithmuller, M. L. 2000 Advances in iterative multigrid PIV image processing, *Exp. Fluids* 29, 51-60.
- Sharland I.J. 1964 Sources of noise in axial flow fans *J. Sound Vib.* 1(3), 302-322.
- Spalart, P. 1988 Direct simulation of a turbulent boundary layer up to  $Re_\theta=1410$ , *J Fluid Mech* 187, 61-98.
- Wallace, J. M., Eckelmann H. & Brodkey R.S. 1972 The Wall Region in Turbulent Shear Flow. *J Fluid Mech.* 54, 39-48.
- Westerweel, J. 1997 Fundamentals of digital particle image velocimetry, *Meas. Sci. Tech.* 8, 1379-1392.